Chapter III

Enhancement of Orientational Order Parameter of Nematic Liquid Crystals in Thin Cells

3.1 Introduction

In the previous chapter we have seen that the application of strong electric fields on the compounds with both $\Delta\varepsilon > 0$ as well as $\Delta\varepsilon < 0$, enhances the orientational order parameter in the nematic phase and the paranematic-nematic transition temperature is shifted to higher values. These effects have contributions both from the Kerr effect as well as from the quenching of director fluctuations under strong fields. Our experiments on the system with $\Delta\varepsilon < 0$ show that the contribution from the quenching of director fluctuation is rather strong. We have also discussed the surface induced order at zero field, whose effect is seen at a temperature slightly higher than that of the bulk transition.

In this chapter we will discuss the effect of confinement on the orientational order parameter of nematic liquid crystals. Liquid crystals can be confined in different geometries. In a simple geometry the liquid crystal is sandwiched between two parallel glass plates, which are pretreated for homogeneous alignment. Such studies on nematic liquid crystals are important both from fundamental and technological points of view. For example, nematic liquid crystal is sandwiched between two parallel glass plates for display (LCD) applications. The typical thickness used for this purpose is ~5μm. In the reflective mode displays, it is about 2μm. Because of the fluid nature of the medium its response time is relatively slow and is given by $\tau = \eta\, d^2/\pi^2 K$ [1] where η is an effective viscosity, K an effective curvature elastic constant and d the sample thickness. The response time can be reduced considerably by reducing the sample thickness. Furthermore, in bistable displays, which are being investigated in recent years, the thickness has to be quite small, ~ 2μm [2].

There are several theoretical and a few experimental studies on the confinement effect on the orientational order parameter of nematic liquid crystals [3-7,9]. Ping Sheng

has calculated the order parameter profile in thin cells using the Landau de Gennes theory assuming a surface potential, which enhances the order parameter at the surface. The dimensionless surface potential g is defined as $G/(A\xi_0 aT_{NI})$, where G is the strength of the surface potential, A is the surface area and a is a Landau coefficient (see section 3.5) and ξ_0 the order parameter coherence length. It was found that within a limited range of surface potentials a surface transition occurs at a temperature higher than that of the bulk transition (Fig.(3.1)). Close to the transition point, the surface induced order decays to the bulk value over a length scale, which is an order of magnitude larger than the order parameter correlation length ξ_0 [3,4]. The order parameter in the nematic phase at the surface of the substrate as well as in the bulk increases with decreasing cell thickness. The calculated surface and bulk order parameter profiles are shown in Fig.(3.1).(adapted from reference [3])

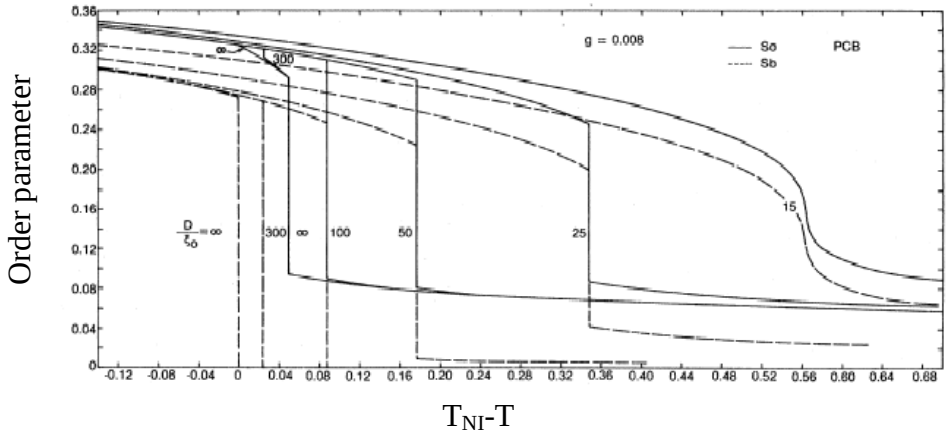

Figure 3.1: Variations of bulk order parameter S_b (dashed curve) and surface order parameter S_0 (solid curve) as functions of temperature (T_{NI}-T). The half-cell thickness (D/ξ_0) of the sample is labelled beside each curve. The magnitude of the dimensionless surface potential g which was defined by Ping Sheng [3] was taken to be 0.008 in the calculations.

Experimentally Miyano [5] measured the wall-induced birefringence in 5CB above the N-I transition temperature. It was found that the pretransition birefringence diverges when the plates were pretreated for homeotropic alignment of the director. However he did not find any evidence for this in planar alignment. Mada et al [6]

reported the measurement of surface and bulk order parameters in the nematic as well as in the isotropic phase as functions of temperature. They used plates, which were pretreated by oblique evaporation of SiO. The surface order parameter was found to be ~0.15 just above T_{NI} and had finite values even at temperatures further above T_{NI}. In the nematic phase the surface order parameter was found to be always ~25% higher than the bulk order parameter. As we have discussed in the previous chapter, the surface induced order becomes measurable in the compound used at ~0.05^0C above the bulk transition temperature and it grows as the temperature is lowered to the transition point.

Experimental measurement of Δn on 8OCB as a function of temperature at different cell thicknesses was reported by Marcerou et at [7]. The measurements were made in cells in which the glass plates were pretreated with polyimide and rubbed unidirectionally. The birefringence ($\Delta n \propto S$, where S is the orientational order parameter) measured in a thin cell was larger at all temperatures than that in a thick cell. For example it was ~30 % larger in a cell of thickness $2.6\mu m$ than that in $7.2\mu m$ thick cell at $T \approx T_{NI}$ - 10^0. They argued that the increase in order parameter was due to an induced biaxial nematic phase in a relatively thick boundary layer (~$0.8\mu m$) even though the medium was uniaxial in the bulk. However the large enhancement (~30 %) for the cell of thickness $2.6\mu m$ may be an experimental artifact [8].

Later Sobha et al [9] reported that Δn is enhanced by a measurable amount in thin cells (~$1.5\mu m$) compared to that in thick cells (~$18\mu m$) in CP7B (p-cyanophenyl p-n heptylbezoate). Interestingly the nematic-nematic (N-N) transition in CP7B, which occurs below the ambient temperature in the bulk is found to shift to higher temperatures in thin cells (~$3\mu m$) (Fig.(3.2a)). When the thickness of the cell is reduced to ~$1.9\mu m$, the N-N transition temperature is increased further by ~4^0C (Fig.(3.2b)). They argue that the shift in the N-N transition temperature is a clear consequence of the significant enhancement of the order parameter as the cell thickness is decreased. Using the Landau de Gennes theory they describe a *uniaxial* nematic made of *biaxial* particles, which gives rise to relatively large value for the correlation length of the order parameter in a suitable parameter range [10]. The large correlation length can give rise to a significant enhancement of the order parameter in thin cells. Recently Manjula et al have confirmed

that in a binary mixture, in which the N-N transition in the bulk occurs above the ambient temperature, the transition temperature increases as the thickness is decreased [11].

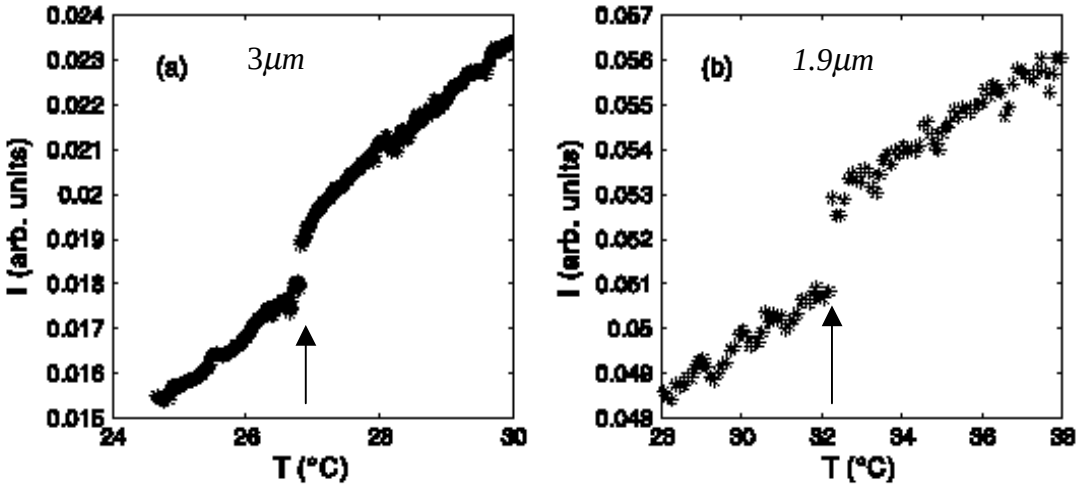

Figure 3.2: Transmitted intensity as a function of temperature for cells of thicknesses of $3\mu m$ and $1.9\mu m$ respectively. (Adapted from ref.[9]). Arrows indicate the jump in the transmitted intensity at the N-N transition. Note that the N-N transition temperature is enhanced by $\sim 4^0$ in the $1.9\mu m$ sample compared to that in the $3\mu m$ cell.

Both the compounds 8OCB and CP7B used in the previous studies have longitudinal dipole moments. In order to check if the enhancement of orientational order parameter in thin cells is a general feature of nematic liquid crystals we have carried out such experiments on systems having both longitudinal and transverse dipole moments.

3.2 Experimental

We have chosen a number of compounds, with dipole moments making different angles with the long axis of the molecule. The chemical structures and phase sequences are given in Fig.(3.3). The first compound (S1014) is obtained from Merck. It is highly polar and the direction of the permanent dipole moment makes a large angle with the long axis and hence the dielectric anisotropy is negative ($\Delta\varepsilon < 0$). The nematic phase occurs over a wide temperature range and can be supercooled to room temperature. It also has a smectic-C like short-range order (cybotactic groups) in the entire nematic range [12]. The

second compound (PCH-5) also obtained from Merck, is highly polar. It exhibits a nematic phase at room temperature and is widely used in display applications.

1.

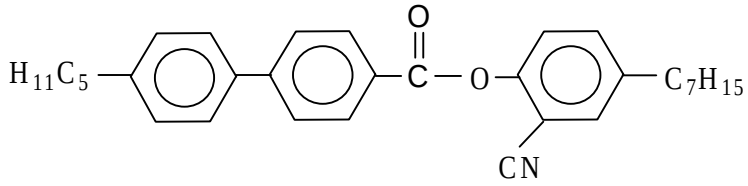

S1014: Cr 45 N 102 I

2.

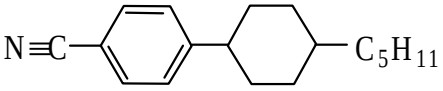

PCH-5: Cr 30 N 55.5 I

3.

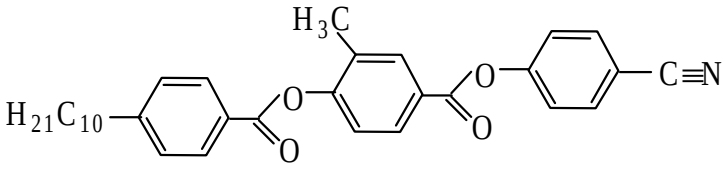

Cr 105.5 N 154.2 I

4.

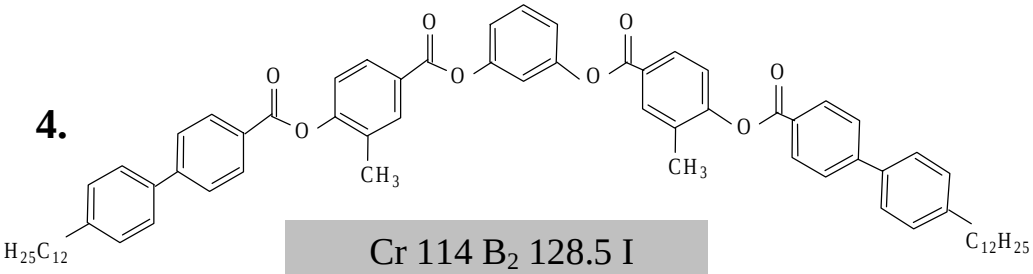

Cr 114 B_2 128.5 I

5.

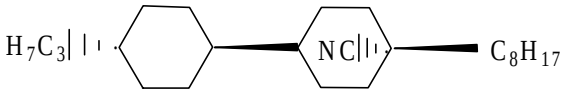

Cr 28 SmA 30.6 N 59.7 I

Figure 3.3: Chemical structures, phase sequences and the transition temperatures of the compounds used in thin cell experiments. The transition temperatures are given in degree Celsius.

The direction of the permanent dipole moment in this molecule is along the long axis and hence the dielectric anisotropy is positive ($\Delta\varepsilon > 0$). The third and fourth compounds are obtained from Prof. B.K. Sadashiva. The third compound is also highly polar with a long alkyl chain. It exhibits the nematic phase at relatively high temperatures. The direction of the permanent dipole moment in this molecule is also along the long axis and hence the dielectric anisotropy is positive ($\Delta\varepsilon > 0$). The fourth compound is made of banana shaped molecules and is highly biaxial. The mixture with 50:50 wt % of the compounds-3 and 4, gives rise to a uniaxial nematic with positive dielectric anisotropy. This mixture was studied to explore the effect of molecular biaxiality on the order parameter. The last compound was used in the high electric field experiments reported in the previous chapter and obtained from Merck. It is highly polar with a negative $\Delta\varepsilon$.

The cell is constructed using two ITO coated glass plates which are etched as shown in Fig.(1.16) of chapter-I. This electrode pattern is designed to perform Freedericksz transition experiments on the systems with $\Delta\varepsilon > 0$. The plates are treated with polyimide and cured at a temperature of 280 ^{0}C for 90 minutes. After curing, the plates are rubbed for homogeneous alignment of the molecules in the nematic phase. Glass beads are mixed with epoxy glue, which is spread outside the electrode region to get the required cell thickness (>2μm). However to make cells of thicknesses < 2μm we do not use any spacers. The glue used does not affect the liquid crystals and is usually used for making liquid crystal displays. The thickness of the cell is measured carefully at several positions inside the overlapped electrode area (see Fig.(1.16)) using an Ocean Optic spectrometer (see Fig.(1.18)). Several cells are made at a time and those with uniform thickness are selected for the experiment. The cell thickness *d* is found to be constant within 1%. To test if the cell thickness changes with temperature, we heated the empty cell up to 150 ^{0}C and measured the thickness at several temperatures and found no noticeable change. The cell is filled with the sample in the isotropic phase by capillary action. The experimental setup is shown in Fig.(3.4). A heating stage (INSTEC HS1) is used to control the temperature to an accuracy of ~10 *mK*. The heater is kept on the rotating stage of a polarizing microscope (Leitz ORTHOPLAN). A helium-neon laser (ORIEL 3 *mW*, λ = 632.8 *nm*) beam is used to illuminate the sample. A beam splitter (BS) and a reference photodiode (PD2) are arranged to monitor the stability of the

reference beam intensity. The laser beam is made to be incident on the sample through a polariser and the transmitted intensity is passed through an analyser, which is crossed with respect to the polariser. The transmitted intensity is collected by the photodiode PD1. The photodiodes are connected to a multimeter. Finally all the instruments are controlled by a computer (COM). A suitable program is used to run the experiment. This setup is only used for Freedericksz transition measurements. To measure the threshold voltage for the Freedericksz transition the temperature is kept fixed and a signal generator is used to apply an electric field to the cell. The transmitted intensity is measured as a function of applied voltage. The typical frequency used in the experiment is 3.111 kHz. The above setup can also be used to measure Δn from the transmitted optical intensity. In thick cells the variation of optical intensity shows maxima and minima as a function of temperature between two crossed polarizers. Using equations (2.43) and (2.44) and using d instead of $2d$, Δn can be measured. However in thin cells ($< 2\mu m$) the variation of optical intensity shows only one broad maximum and hence it is not possible to calibrate the intensity and hence measure Δn accurately. Therefore Δn values in all the cells are

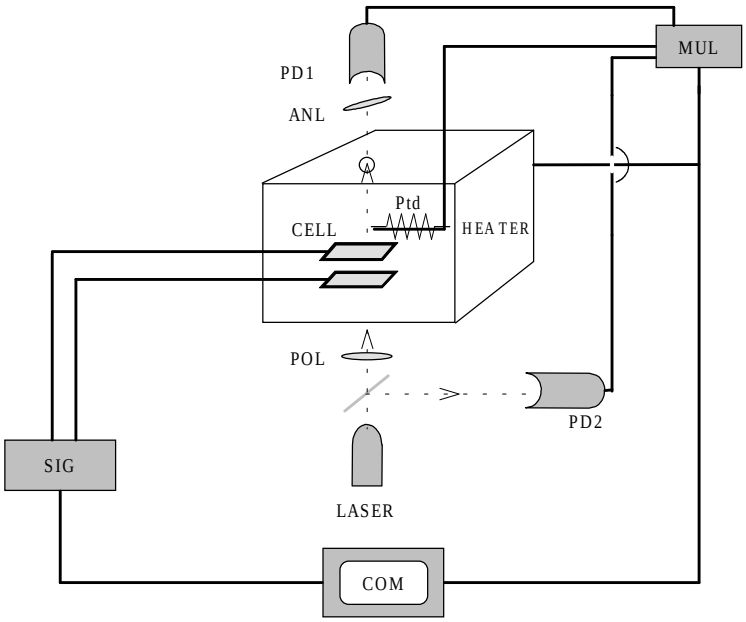

Figure 3.4: Schematic diagram of the experimental setup. Photodiodes (PD1, PD2). Polariser (POL), Analyzer (ANL), Multimeter (MUL), Computer (COM). Signal generator (SIG).

measured by using a tilting compensator (Leitz (5λ)). The measurements are made while cooling the samples from the isotropic phase.

3.3 Results and Discussion

The variations of Δn measured in two cells of thicknesses of $1.5\mu m$ and $6.7\mu m$ are shown as functions of temperature for the compound-1 in Fig.(3.5). The Δn data measured using the tilting compensator in the thick cell compares well with the data of reference [13] (Fig.(3.6)) in which n_e (extraordinary refractive index) and n_o (ordinary refractive index) have been measured separately using a goniometer. Δn measured in the thin cell ($1.5\mu m$) is larger at all temperatures than that in the thick cell ($6.7\mu m$) and at the lower temperatures, the two curves are roughly parallel (Fig.(3.5)). It should be pointed out that the compound-1 has also a smectic-C like short range order throughout the nematic range [12].

The variations of birefringence (Δn) of the compound-2 measured in two cells of thicknesses of $1.4\mu m$ and $7\mu m$ are shown as functions of temperature in Fig.(3.7). Close to the isotropic to nematic transition point ($T_{NI} - T < 2^0$) Δn measured in the two cells are comparable. At lower temperature, there is a clear enhancement in Δn in the thinner cell. For example, it is ~6% higher than in the thicker cell at 5^0 below T_{NI}.

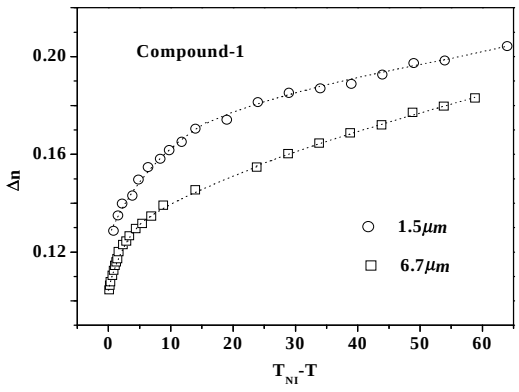

Figure 3.5: Variations of Δn in the compound-1 in $1.5\mu m$ (open circles) and $6.7\mu m$ (open squares) thick cells as functions of temperature. Dotted lines are drawn as guides to the eye.

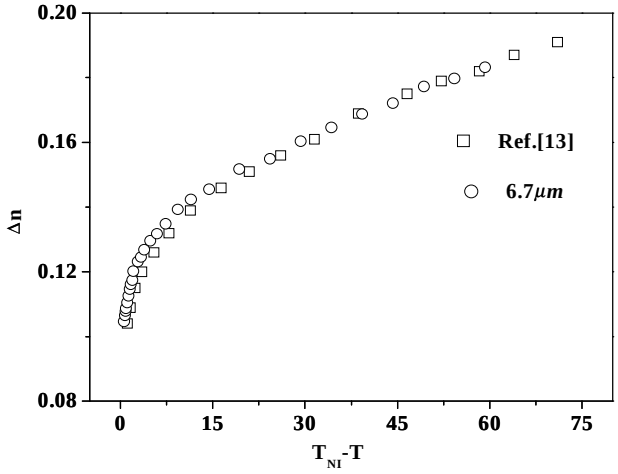

Figure 3.6: Comparison of Δn measured by tilting compensator in the thick cell (6.7μm) (open circles) with the data of Δn (open squares) from ref. [13] of the compound-1.

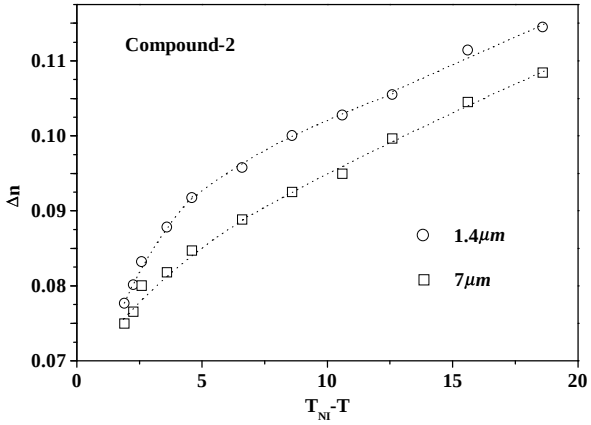

Figure 3.7: Variations of Δn of the compound-2 measured in 1.4μm (open circles) and 7μm (open squares) thick cells as functions of temperature. Dotted lines are drawn as guides to the eye.

The variations of Δn as functions of temperature are shown for cells of three different thicknesses namely 1.5μm, 2.2μm and 14μm for the compound-3 in Fig.(3.8).

This compound exhibits the nematic phase at high temperatures (105.5 to 154.2 ^{0}C). Again, at a fixed temperature, Δn increases with decreasing cell thickness (Fig.(3.8)). For example, at T_{NI} -T =12^0, Δn is higher by ~6 % and ~11 % respectively in the 2.2 μm and 1.5μm cells compared to that in the cell of thickness 14μm. For this compound we analyse the temperature dependence of Δn, which can be approximated well for nematic liquid crystals [14] by the formula

$$\Delta n = \Delta n_0 \left(1 - \frac{T}{T_1}\right)^{\beta} \tag{3.1}$$

where T_1 and β are adjustable parameters. Least squares fits to the experimental data of compound-3 with the equation (3.1) are shown for the three different cell thicknesses in Fig.(3.8). It is noticed that the fitted birefringence Δn_0 of the completely ordered sample in 1.5μm is slightly higher (by ~5%) than that in 2.2 and 14μm cells. The fit parameter T_1

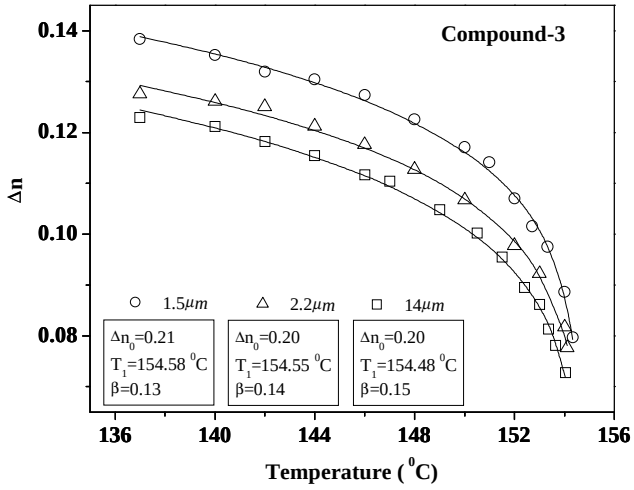

Figure 3.8: Variations of Δn of compound-3 as functions of temperature in cells of three different thicknesses: 1.5μm (open circles) 2.2μm (open triangles), 14μm (open squares). Continuous lines are the theoretical fits to the equation (3.1). The relevant fit parameters are shown in the insets.

is increased by ~0.1^0 in the 1.5μm cell than that in the 14μm cell. This indicates that T_{NI} increases as the thickness is decreased as predicted by the Landau theory (see Fig.(3.1)) and hence T_1 which is slightly above T_{NI} is also increased. However our main interest is to study the effect of confinement on the orientational order parameter and we have not carefully measured the enhancement of T_{NI} at reduced thicknesses of the samples. The value of β is 0.13 in the 1.5μm thin cell and increases to 0.15 in the 14μm thick cell. Similar values of β are obtained in several other nematics as discussed in the previous chapter.

The variations of Δn in the 50:50 wt% mixture of the compounds-3 and 4 are shown as functions of temperature in Fig.(3.9) for three thicknesses. Close to the transition temperature the data points are noisy because this mixture exhibits a nematic-isotropic coexistence range of ~1 ^{0}C. Therefore in this mixture Δn is measured while heating the sample. Again, at a fixed temperature, Δn increases with decreasing cell thickness. For example at T_{NI}-T =12^0, Δn is higher by ~6 % and ~13 % respectively in the 2.3 μm and 1.4μm cells compared to that in the cell of thickness 16μm.

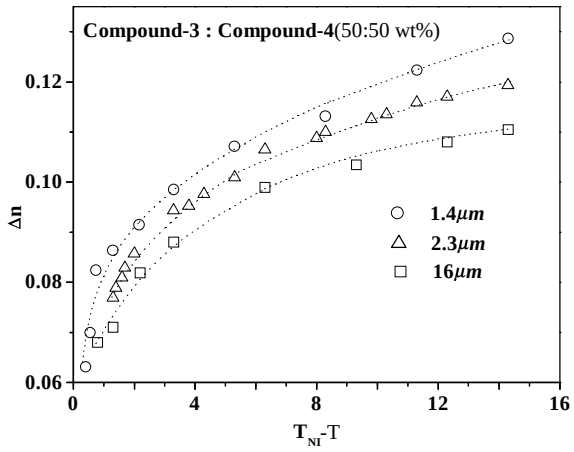

Figure 3.9: Variations of Δn as functions of temperature of the mixture of compounds-3 and 4 in three different cell thicknesses namely 1.4μm (open circles) 2.3μm (open triangles), 16μm (open squares). Dotted lines are drawn as guides to the eye.

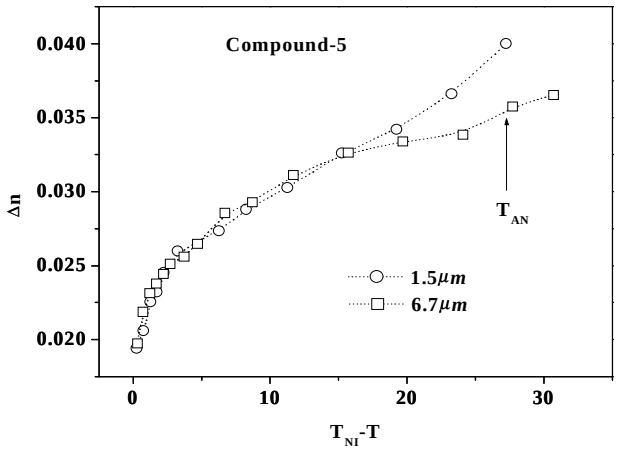

Figure 3.10: Variations of Δn of compound-5 in ~1.5μm (open circles) and ~6.7μm (open squares) cells as functions of temperature. Note that the separation between the two curves increases as T_{AN} (smectic to nematic transition temperature) is approached. Dotted lines are drawn as guides to the eye.

The variations of Δn as functions of temperature are shown for the compound-5 in two different cell thicknesses namely 1.5μm and 6.7μm in Fig.(3.10). The high electric field experiments on this compound described in the previous chapter were conducted using SiO coated plates to get homogeneous alignment of the sample. In the present studies rubbed polyimide coated glass plates are used for alignment. Interestingly no significant difference is noticed between the two curves corresponding to the two thicknesses in the nematic phase down to T_{NI}-T~20^0. However, when the nematic to smectic-A transition temperature (T_{AN}) is approached, Δn starts to increase in the 1.5μm cell. There is an enhancement of Δn in both the cells as the temperature approaches T_{AN}, and the relative enhancement in the thinner cell also grows. For example, at T_{AN} the Δn in thinner cell is ~10% higher than that in the thicker cell.

We summarise the experimental results of Δn on all the five systems studied in Table-I. The relative enhancement of (Δn) in thin cells with respect to thick cells is also shown in Table-I. We notice that in the first four systems Δn is enhanced considerably in thin cells than that in the thick cells. It is also noticed from the table that due to the

addition of biaxial molecules in the mixture, the enhancement of Δn in thin cells does not change significantly from that of the compound-3. Thus the effect of molecular biaxiality on the orientational order parameter in thin cells is not significant.

Table-I

Compounds	Thicknesses of thin and thick cells	$(T_{NI} - T)$ °	$\frac{\Delta n_{thin} - \Delta n_{thick}}{\Delta n_{thick}} \times 100$
Compound-1	1.5 and 6.7μm	12	15 %
Compound-2	1.4 and 7μm	12	6 %
Compound-3	1.5 and 14μm	12	11 %
Mixture (50:50 wt%)	1.4 and 16μm	12	13 %
Compound-5	1.5 and 6.7μm	12	No significant difference

We have also measured the threshold voltage for Freedericksz transition of the materials with positive dielectric anisotropy. The same cell in which Δn is measured is used to measure V_{th}. Typical frequency used for the experiment is 3111 Hz. The threshold voltage of the Freedericksz transition is given by $V_{th} = \pi\sqrt{K_1 / \varepsilon_0 \Delta\varepsilon}$, where K_1 is the splay elastic constant and $\Delta\varepsilon$ is the dielectric anisotropy. In the mean field model the elastic constant, $K_1 \propto S^2$ where S is the orientational order parameter and the dielectric anisotropy $\Delta\varepsilon \propto S$. Therefore $V^2{}_{th} \propto S$. As we can see from Fig.(3.11), $V^2{}_{th}$ is higher in 1.4μm cell than that in 7μm cell of the compound-2. V_{th}^2, measured in three different cells of the compound-3 are shown at a few temperatures in Fig.(3.12). Similarly $V^2{}_{th}$ for the mixture are shown at a few temperatures in Fig.(3.13). It is observed that with decreasing cell thickness $V^2{}_{th}$ is increased at a fixed temperature. We summarise the experimental results of V_{th}^2 in Table-II.

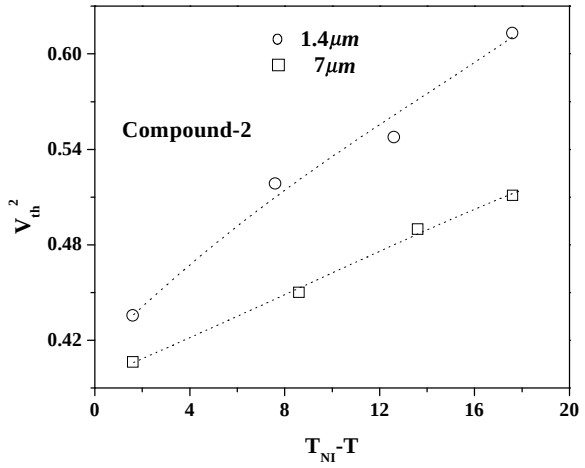

Figure 3.11: V_{th}^2 at a few temperatures of the compound-2. The open circles and open squares correspond to 1.4 μm and 7μm thick cells respectively. Dotted lines are drawn as guides to the eye.

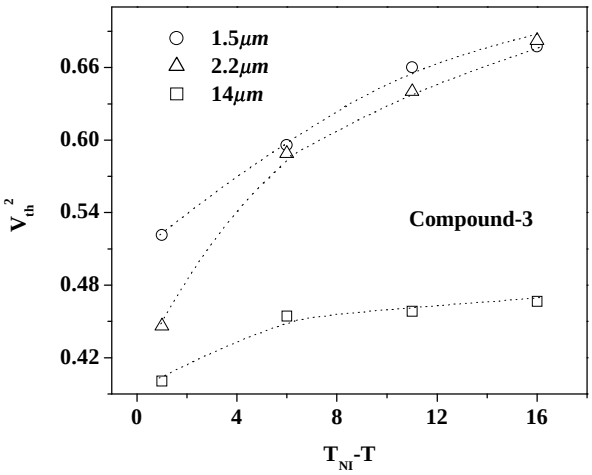

Figure 3.12: V_{th}^2 at a few temperatures in three different cells of the compound-3. Open circles (1.5μm), open triangles (2.2μm), open squares (14μm),. Dotted lines are drawn as guides to the eye.

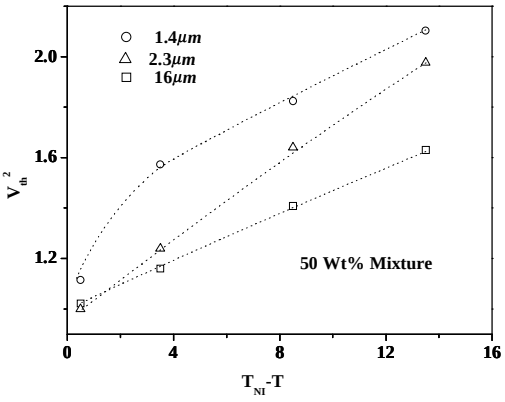

Figure 3.13: V_{th}^2 at a few temperatures in three different cells of the mixture. Open circles (1.4μm), open triangles (2.3μm), open squares (16μm). Dotted lines are drawn as guides to the eye.

Table-II

Thicknesses of thin and thick cells	Compounds	$(T_{NI}-T)^0$	$\frac{\Delta n_{thin} - \Delta n_{thick}}{\Delta n_{thick}} \times 100$	$\frac{\left(V_{th}^2\right)_{thin} - \left(V_{th}^2\right)_{thick}}{\left(V_{th}^2\right)_{thick}} \times 100$
1.4 and 7μm	Compound-2	12	6%	16%
1.5 and 14μm	Compound-3	12	11%	43%
1.4 and 16μm	Mixture (50:50 wt%)	12	13%	30%

In the compound-2, V_{th}^2 is ~16 % larger in 1.4μm cell than that in 7μm cell at ~12^0 below T_{NI} whereas Δn is ~6% larger at the same temperature. In the compound-3, V_{th}^2 is ~43% larger in 1.5μm than that in 14μm cell whereas Δn is ~11 % larger at the same temperature. Similarly in the mixture V_{th}^2 is 30% larger in 1.4μm cell than that in 16μm cell whereas Δn is ~13% larger at the same temperature. These discrepancies can be explained as follows. All the samples have ionic impurities. The transit time ($t = d^2/\mu V$,

where μ, is the mobility) of the impurity ions in the thin cells is small and hence the ions can easily reach the appropriate electrodes when the field is reversed, producing a space charge. The space charges screen the external electric field. Therefore the effective field inside the thin cells is decreased. The large excess value of V_{th}^2 in thin cell arises due to the screening effect of the space charge apart from the enhancement of *S*. It is also noticed from the Table-II that in the compound-2 and in the mixture the enhancement of V_{th}^2 in thin cells is ~2.5 times larger than that of Δn whereas this is ~ 4 times larger in compound-3. In this compound the nematic phase occurs at high temperatures (105.5-154.2^{0}C). The density of ions increases with the increase of temperatures and as a result the screening effect is increased. In the next chapter we will discuss the effect of space charge polarisation in thin cells in detail.

The orientational order parameter in thin cells in the first four systems studied is considerably larger compared to that in the thick cells irrespective of the molecular structure, temperature range and orientation of the permanent dipole moments in the molecules. Compound-5 has no aromatic rings and also does not exhibit any significant dependence of Δn on the thickness.

To understand the enhancement of the orientational order parameter in thin cells two possibilities can be invoked: (a) suppression of the thermal fluctuations of the director in thin cells can enhance the order parameter compared to the thicker cell, (b) larger effect of surface-order increasing the measured Δn in thin cells. First we will discuss the effect of thermal fluctuations of the director on the magnitude of the scalar order parameter in thin cells.

3.3.1 Quenching of Director Fluctuations in Thin Cells

In the nematic phase there are thermal fluctuations of the director as discussed in the previous chapter. In the one elastic constant approximation the fluctuation amplitude is given by [1]

$$\left\langle \left| n(q) \right|^2 \right\rangle = \frac{k_B T}{VKq^2} \tag{3.2}$$

where k_B is the Boltzmann constant, T the temperature, V the volume, and K is the elastic constant. The wave vector $\vec{q}$, can be decomposed into q_z, along the z axis and $q_\perp$, which is in the xy plane (Fig.(3.14)). A pictorial representation of a few fluctuation modes with allowed values of q_z are shown in Fig.(3.14). Any mode which has wavelength $(2\pi/q_z)$ larger than twice the cell thickness d is not allowed, due to the confinement along the z direction. We have discussed in the previous chapter that a stabilizing electric field also quenches the director fluctuations. In that case the fluctuation amplitude is reduced but the number of modes remain the same. In the present situation the number of modes are reduced when the thickness is decreased.

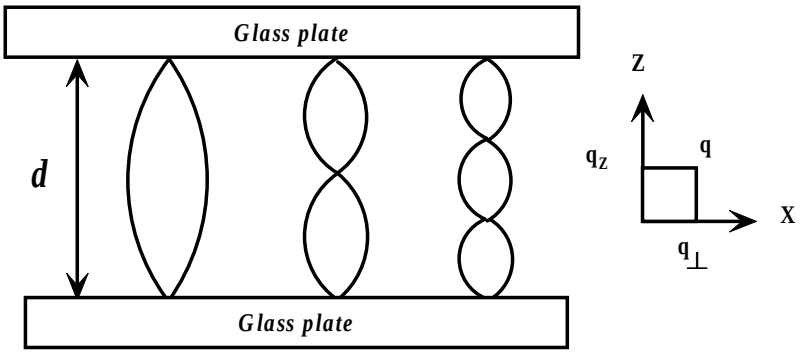

Figure 3.14: Schematic representation of a few allowed fluctuation modes between the two plane surfaces.

In principle, to calculate the r.m.s. fluctuation in real space, we have to sum over the allowed modes along the z direction (Fig.(3.14)) [15]. However, as the smallest gap d used in our experiment is $>1\mu m$ which is much larger than the intermolecular distance a ($\approx 2\times10^{-7}$cm), we will replace the summation by an integration over the appropriate limits. In real space the fluctuation amplitude is given by

$$\left\langle \left|n_\perp(r)\right|^2 \right\rangle = \frac{k_B T}{8\pi^3 K} \int_{\pi/d}^{q_{max}} dq_z \int_0^{q_{max}} \frac{2\pi q_\perp dq_\perp}{q_\perp^2 + q_z^2} \tag{3.3}$$

where $q_{max} \approx 2\pi/a$,is the cut off wave vector. Integrating over $q_\perp$ we get,

$$\left\langle \left| n_{\perp}(r) \right|^2 \right\rangle = \frac{k_B T}{8\pi^2 K} \int_{\pi/d}^{q_{\max}} \left[\ln\left(1 + \frac{q_{\max}^2}{q_z^2} \right) \right] dq_z \,. \tag{3.4}$$

As $d \approx 1\mu m$, $q_{\max} d \approx 10^3$. We use this to simplify the above integral to get

$$\left\langle \left| n_{\perp}(r) \right|^2 \right\rangle \approx \frac{k_B T}{8\pi^2 K} \left[q_{\max} \left(\ln 2 + \frac{\pi}{2} \right) + \frac{2\pi}{d} \left\{ \ln\left(\frac{\pi}{d q_{\max}} \right) - 1 \right\} \right] . \tag{3.5}$$

It is noticed from equation (3.5) that the fluctuation amplitude is reduced with the reduction of the sample thickness. Using equation $\left\langle n_z^2 \right\rangle = 1 - 2\left\langle n_{\perp}^2 \right\rangle$, and $S = \left[\frac{3}{2} \left\langle n_z^2 \right\rangle - \frac{1}{2} \right]$ we get the order parameter in a finite thickness cell d as $S_d = 1 - 3\left\langle \left| n_{\perp}(r) \right|^2 \right\rangle$. Using equation(3.5) the order parameter S_d can be written as

$$S_d = 1 - \frac{3k_B T}{8\pi^2 K} \left[q_{\max} \left(\ln 2 + \frac{\pi}{2} \right) + \frac{2\pi}{d} \left\{ \ln\left(\frac{\pi}{d q_{\max}} \right) - 1 \right\} \right]. \tag{3.6}$$

Using K=5×10^{-7} dynes, a = 10 $\overset{0}{A}$, and T=373K, we find that the order parameter increases by ~0.1% in 1μm cell compared to that in 10μm cell. On the other hand experimentally we find in the first four compounds (see Table-I) the enhancement of order parameter in thin cells (~1.4μm) is nearly 6 to13% compared to that in the thick cells (~10 -15μm). As such the enhancement of order parameter due to the partial quenching of the director fluctuations in thin cells can not explain our experimental result.

Now we consider the effect of confinement on the order parameter of nematic liquid crystals due to the alignment at the walls. We have discussed in section 3.1 that using the Landau de Gennes theory Ping Sheng calculated the order parameter profile in thin cells [3,4]. He restricted the calculation between T_{NI} -0.12^0 to T_{NI} +0.36^0. We extend the calculation to few degrees below T_{NI} to see the effect of confinement on the order parameter.

3.3.2 Landau de Gennes Theory of a Nematic Liquid Crystal Confined Between Two Plane Parallel Plates with a Large Surface Orientation Potential

We consider a nematic liquid crystal confined between two plane parallel surfaces separated by *d*. The solid-liquid crystal interfaces are defined by *z = 0* and *z = d* (Fig.(3.14)). The sample is assumed to be uniform in *x* and *y* directions. The substrates are treated such that the molecules experience a uniaxial aligning potential in a particular direction. For example let us assume that the alignment direction is along the *x*-axis (Fig.(3.14)). The surface potential felt by each molecule can be expressed in general as [3]

$$\upsilon(\theta, z) = -G\delta(z)\left[P_2(\cos\theta) + bP_4(\cos\theta) + cP_6(\cos\theta).....\right] \tag{3.7}$$

where θ is the angle between the long axis of the molecule and $\hat{n}$. *G* is a constant which denotes the strength of the surface potential, P_{2n} are the even order Legendre polynomials, and *b*, *c* are expansion coefficients for the angular part of the surface potential [3]. In equation (3.7) it is assumed that the surface potential is short range as indicated by the delta function. For simplicity of the calculation the series expansion of the potential can be restricted to the first term and the macroscopic potential averaged over many molecules over a small volume is given by

$$V = \langle \upsilon(\theta, z) \rangle = -G\delta(z)\langle P_2(\cos\theta) \rangle = -G\delta(z)S \tag{3.8}$$

where the angular brackets represent a local average. As we have experimentally found that the enhancement of order parameter in thin cells is very substantial, we assume the surface potential is so large that there is perfect order at the surface i.e. $S(d) = S(0) = 1$. Selinger et al [16] calculated the variation of order parameter from the surface to the bulk assuming a strong surface potential (V_S=10V_0, where V_0 is the Maier-Saupe orientation potential between the molecules) as discussed in the last chapter. It was found that at the surface the order parameter is saturated i.e. $S(0) = 1$(see Fig.(2.31)). However, they did not extend the molecular theory to the nematic phase.

The Landau-de Gennes free energy density is given by [4]

$$\varphi = f(S) + L\left[\frac{dS}{dz}\right]^2 \tag{3.9}$$

where $$f(S) = \frac{a}{2}(T - T^*)S^2 - \frac{B}{3}S^3 + \frac{C}{4}S^4. \quad (3.10)$$

$f(S)$ is the bulk free energy density and *a*, T^* *B, C* are material parameters. *L* is the bare elastic constant. For a given φ, the total free energy per unit area (Φ / A) is obtained directly by integrating over *z*:

$$\frac{\Phi}{A} = \int_0^d \left[f(S) + L\left[\frac{dS}{dz}\right]^2 \right] dz. \quad (3.11)$$

The Euler–Lagrange equation for the minimization of (Φ / A) is given by

$$\frac{\partial \varphi}{\partial S} = \frac{\partial}{\partial z}\left(\frac{\partial \varphi}{\partial\left(\frac{\partial S}{\partial z}\right)} \right) \quad (3.12)$$

Using equations (3.9) and (3.10) we get,

$$\frac{\partial f(S)}{\partial z} = 2L\left(\frac{d^2 S}{dz^2}\right)\left(\frac{dS}{dz}\right). \quad (3.13)$$

Equation (3.13) can be integrated once to get

$$L\left(\frac{dS}{dz}\right)^2 = f(S) + C \quad (3.14)$$

where *C* is an integration constant and can be determined by the following boundary conditions [4]

$$S = 1 \quad \text{at} \quad z = 0, d$$
$$\left[\frac{dS}{dz}\right]_{z = d/2} = 0, \quad \text{and} \quad S\left(d/2\right) = S_m, \quad (3.15)$$

S_m is the minimum order parameter which is obtained at the mid-plane of the sample. Using the above boundary conditions in equation (3.14) we get,

$$L\left(\frac{dS}{dz}\right)^2 = f(S) - f(S_m). \quad (3.16)$$

Dividing both sides by aT_{NI}, we get a dimensionless equation, which is given by

$$\xi_0^2\left(\frac{dS}{dz}\right)^2 = F(S) - F(S_m) \quad (3.17)$$

where $\xi_0 \equiv \sqrt{\frac{L}{aT_{NI}}}$, is the bare correlation length and $F(S)=\frac{f(S)}{aT_{NI}}$ and $F(S_m)=\frac{f(S_m)}{aT_{NI}}$.

The *S*(z) profile can be obtained easily by integrating equation (3.17)

$$\frac{z}{\xi_0} = \int_{S(z)}^{1} \sqrt{\frac{1}{F(S)-F(S_m)}}\ dS\,. \tag{3.18}$$

The material parameters *a, B, C* for compound-2 are assumed to be *a* = 0.10 J/cm^3-*K*, *B* = 1.5 J/cm^3, *C* = 3.8 J/cm^3, T^* = 327.2 *K*, T_{NI} = 328.5 *K*. The first three coefficients are of the same order as in other nematics [3]. The elastic constant *L*, is found by using the formula [18]

$$L = \frac{1}{2}\left[\frac{K_1 + K_2 + K_3}{3S^2}\right] \tag{3.19}$$

where K_1, K_2 and K_3 are the splay twist and bend elastic constants and taken from reference [19]. *L* is estimated to be ~3×10^{-13} *J/cm*. The estimated bare coherence length ξ_0~10 $\overset{0}{A}$. Using these parameters we have numerically calculated *S*(z) profile for half the cell thickness at a few temperatures in the nematic phase. The variation of calculated $S(z)$ at $T_{NI}-1^0$ is shown as a function of z/ξ_0 in Fig.(3.15). It is noticed that the surface order parameter decays to the value of S_m in z/ξ_0 ~50. The thickness averaged order parameter is calculated by integrating $S(z)$,

$$\bar{S} = \frac{1}{d}\int_0^d S(z)\ dz\,. \tag{3.20}$$

We can introduce an additional elastic term $L'\left[S\frac{dS}{dz}\right]^2$ in equation (3.9) where L' is also an elastic constant. This term is also allowed by the symmetry of the medium. Following a procedure similar to that given above and assuming $L = L'$, we find

$$\frac{z}{\xi_0} = \int_{S(z)}^{1} \sqrt{\frac{1+S^2}{F(S)-F(S_m)}}\ dS\,. \tag{3.21}$$

Using the same material parameters *a, B, C,* T^* we calculate the variation of order parameter $S^*(z)$ at a few temperatures. The order parameter, $S^*(z)$ profile which is calculated at $T_{NI}-1^0$ including $L(S\partial S/\partial z)^2$ term in equation (3.9) is shown by a dotted

line in Fig.(3.15). We notice that the over all variation of $S^*(z)$ is similar to that of $S(z)$. The order parameter $S^*(z)$ is somewhat higher between z/ξ_0 =0 to 50 than that of $S(z)$. We summarise the calculated enhancement of order parameter in the 1μm cell at a few temperatures in Table-III.

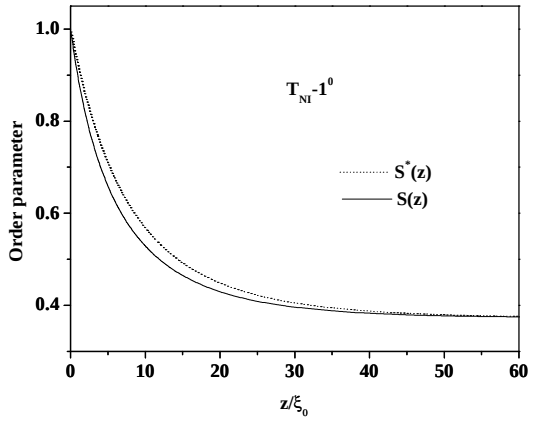

Figure 3.15: Variations of the calculated order parameter $S(z)$(continuous line) and $S^*(z)$(dotted line) as functions of z/ξ_0 for half-cell thickness in the thin cell. Variations are shown only up to z/ξ_0=60 for clarity. [1μm corresponds to $z/\xi_0 = 1000$]

$\bar{S}$ in the 1μm thin cell at $T_{NI} - 0.2^0$ is found to be ~0.310 (see Table-III), whereas the calculated order parameter (S_b) in the bulk is ~ 0.297. Thus in the 1μm thick cell the order parameter is ~4.4% higher than the bulk value at $T_{NI} - 0.2^0$. The calculated enhancement is reduced at lower temperatures. The enhancement is ~2.7% and 0.9% at T_{NI} -1^0 and $T_{NI} - 5^0$ respectively. The thickness averaged order parameter $\bar{S}^*$ at $T_{NI} - 0.2^0$ is ~5.2% higher than the bulk value. $\bar{S}^*$ is slightly higher (~0.8%) than $\bar{S}$ at the same temperature. The calculated enhancement is again reduced at lower temperatures. It is ~3.2% and 1.1% at T_{NI} -1^0 and $T_{NI} - 5^0$ respectively.

Table-III

Temperature	S_b	$\bar{S}$	$\bar{S}^*$	$\frac{\bar{S}-S_b}{S_b}\times 100$	$\frac{\bar{S}^*-S_b}{S_b}\times 100$
$T_{NI}-0.2^0$	0.297	0.310	0.313	4.4%	5.2%
$T_{NI}-1^0$	0.373	0.383	0.385	2.7%	3.2%
$T_{NI}-5^0$	0.566	0.571	0.572	0.9%	1.1%

On the other hand, experimentally, we find that the enhancement is not so drastically reduced at lower temperatures (see Table-I). The Landau de Gennes theory for uniaxial nematic can thus only partially account for the enhancement of order parameter in thin cells (~1μm) close to the nematic- isotropic transition temperature.

Now we discuss the effect of weak biaxiality in the thin cell due to asymmetric director fluctuations.

3.3.3 Confinement Induced Biaxiality

As we have discussed, in thin cells the director fluctuations are partially suppressed in a plane (*yz*) perpendicular to the plates (Fig.3.14). But the fluctuations in the plane (*xy*) of the plates remain unaffected. The asymmetric director fluctuations in the two different planes could lead to a weak biaxiality in the medium [15] if the three elastic constants are different. We use the tensor order parameter to be able to describe this. Considering up to the fourth order term in the expansion, the Landau-de Gennes free energy densities F_b and F_k, [20] can be written as

$$F_b = \frac{A}{2}TrQ_{ij}^2 + \frac{B}{3}TrQ_{ij}^3 + \frac{C}{4}TrQ_{ij}^4 \tag{3.22}$$

$$F_k = L_1\frac{\partial Q_{ij}}{\partial x_k}\frac{\partial Q_{ij}}{\partial x_k} + L_2\frac{\partial Q_{ij}}{\partial x_j}\frac{\partial Q_{ik}}{\partial x_k} + L_3\frac{\partial Q_{ij}}{\partial x_k}\frac{\partial Q_{ik}}{\partial x_j} \tag{3.23}$$

where A (= a (T-T^*)), B, C are the Landau coefficients, which will be numerically different from those in equation (3.10). L_1, L_2, L_3 are the elastic constants and the

summation convention is assumed. The order parameter Q_{ij} is given by a traceless symmetric tensor

$$Q_{ij} = \begin{bmatrix} \frac{-S-P}{2} & 0 & 0 \\ 0 & \frac{-S+P}{2} & 0 \\ 0 & 0 & S \end{bmatrix} \tag{3.24}$$

where S is the usual order parameter and P is the biaxial order parameter. Using equations (3.22), (3.23) and (3.24) we get

$$F_b = \frac{A}{4}\left(3S^2 + P^2\right) + \frac{B}{4}\left(S^3 - SP^2\right) + \frac{C}{16}\left(9S^4 + 6S^2P^2 + P^4\right). \tag{3.25}$$

We assume that the order parameters depend only on z, and $L_1 = L$ and $L_2 + L_3 = 3L$ [19] then equation (3.23) can be simplified as,

$$F_k = \frac{9}{2}L\left(\frac{\partial S}{\partial z}\right)^2 + \frac{L}{2}\left(\frac{\partial P}{\partial z}\right)^2. \tag{3.26}$$

The total free energy density energy is given by

$$F_t = F_b + F_k. \tag{3.27}$$

The Euler-Lagrange equations for minimization of F_t are given by

$$\frac{\partial}{\partial z}\left[\frac{\partial F_t}{\partial\left(\frac{\partial S}{\partial z}\right)}\right] - \frac{\partial F_t}{\partial S} = 0 \tag{3.28a}$$

and

$$\frac{\partial}{\partial z}\left[\frac{\partial F_t}{\partial\left(\frac{\partial P}{\partial z}\right)}\right] - \frac{\partial F_t}{\partial P} = 0. \tag{3.28b}$$

From equation (3.28a) and (3.28b) we get two coupled differential equations

$$9L\frac{\partial^2 S}{\partial z^2} = \frac{3}{2}AS + \frac{B}{4}\left(3S^2 - P^2\right) + \frac{C}{4}\left(9S^3 + 3SP^2\right) \tag{3.29a}$$

$$L\frac{\partial^2 P}{\partial z^2} = \frac{1}{2}AP - \frac{B}{2}SP + \frac{C}{4}\left(3S^2P + P^3\right) \tag{3.29b}$$

Dividing both sides of equation (3.29a) by $9aT_{NI}$ and equation (3.29b) by aT_{NI} we get

$$\xi_0^{\,2}\frac{\partial^2 S}{\partial z^2}=\frac{1}{9aT_{NI}}\left[\frac{3}{2}AS+\frac{B}{4}\left(3S^2-P^2\right)+\frac{C}{4}\left(9S^3+3SP^2\right)\right] \tag{3.30a}$$

$$\xi_0^{\,2}\frac{\partial^2 P}{\partial z^2}=\frac{1}{aT_{NI}}\left[\frac{1}{2}AP-\frac{B}{2}SP+\frac{C}{4}\left(3S^2P+P^3\right)\right] \tag{3.30b}$$

where $\xi_0^{\,2}=L/aT_{NI}$. We assume the following boundary conditions:

$$S(0)=1 \text{ at } z=0 \tag{3.31}$$

$$\frac{dS}{dz}=0 \text{ at } z=d/2$$

$$P(0)=0.5 \text{ at } z=0$$

$$\frac{dP}{dz}=0 \text{ at } z=d/2.$$

The surface treatment is assumed to lead to a very strong biaxial alignment of the molecules at the surface. Using the above boundary conditions, equations (3.30a) and (3.30b) are solved numerically. The material parameters are rescaled as a = 0.07 J/cm^3-K; B = -2.0 J/cm^3; C = 1.7 J/cm^3 and $\xi_0 \sim 11\overset{0}{A}$. The variation of $S(z)$ and $P(z)$ at T_{NI}-1^0 is shown in Fig.(3.16). It is noticed from the Fig.(3.16) that the induced biaxial order parameter $P(z)$ decays to zero within $z/\xi_0 \sim 5$. Calculating the area under the curve of $S(z)$ we find that the enhancement of orientational order parameter is ~ 3% at $T_{NI}-1^0$ and ~1% at $T_{NI}-5^0$. Therefore the effect of induced biaxiality on the measured order parameter is not significant.

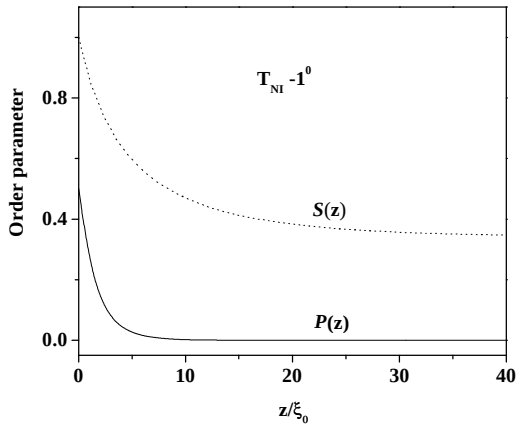

Figure 3.16: Variations of S(z) and P(z) as functions of z/ξ_0 at T_{NI}-1^0 (only up to z/ξ_0=40 is shown for clarity).

We recall that in the compound-5 there is no significant enhancement of order parameter. There is no aromatic core in this compound and the surface potential appears to be extremely small on the polyimide coated surface and hence the enhancement of order parameter at the surface is not significant. However as T_{AN} is approached from the nematic phase the smectic like short-range order appears and the order parameter increases in both the cells. In thin cell the large enhancement of order parameter close to T_{AN} might reflects on the enhancement of smectic short-range order in thin cells.

3.4 Conclusions

Our experiments confirm that the orientational order parameter of nematic liquid crystals in thin cells is enhanced considerably with respect to that in thick cells in all the compounds with aromatic cores. This probably means that the surface orientating potential in these cases is quite strong. Quenching of director fluctuations in thin cells enhances the order by a very small amount ~0.1%. The usual Landau de Gennes theory for the uniaxial medium partially accounts for the enhancement of the order parameter if the surface potential produces perfect order. The predicted enhancement is ~5% at $T_{NI} - 0.2^0$. However, at lower temperatures the calculated enhancement is reduced drastically. In compound-2, which has only one phenyl ring, the relative enhancement is

smaller than in the other compounds with more than one phenyl ring. Indeed in compound-5, which has no phenyl rings in the molecular structure, the surface potential on the aromatic polyimide coating can be expected to be very small. This accounts for the absence of any enhancement in this case. Induced biaxiality also does not improve upon the uniaxial results. Further theoretical study is required to understand the large (~10%) enhancement of order parameter in thin cells even at $T_{NI} - 10^0$.

References:

[1] P. G. de Gennes and J. Prost, " The Physics of Liquid Crystals.," 2nd ed. (Clarendon, Oxford, 1993).

[2] T. Z. Qian, Z. L. Xie, H. S. Kwok and P. Sheng, " Dynamic flow and switching bistability in twisted nematic liquid crystal cell.", Appl. Phys. Lett. **71**, 596 (1997).

[3] P. Sheng, "Boundary-layer phase transition in nematic liquid crystals.," Phys. Rev. A, **26**, 1610 (1982).

[4] P. Sheng, "Phase transition in surface aligned nematic.," Phys. Rev. Lett. **37**, 1059 (1976).

[5] K. Miyano, "Wall-induced pretransitional birefringence: a new tool to study boundary aligning forces in liquid crystals.," Phys. Rev. Lett. **43**, 51 (1979).

[6] H. Mada and S. Kobayashi, " Surface and bulk order parameter of a nematic liquid crystal.," Appl. Phys. Lett. **35** (1), 4 (1979).

[7] F. Beaubois and J. P. Marcerou, " Biaxial nematic and smectic-A boundaries in thin planar samples of 8OCB aligned by rubbed polyimide.," Europhys. Lett. **36,** (2), 111 (1996).

[8] Personal communication from J. P. Marcerou.

[9] R. W. Sobha, D. Vijayaraghavan and N. V. Madhusudana, “Evidence for a nematic to nematic transition in thin cells of highly polar compound.,” Europhys. Lett. **44,** (3), 296 (1998).

[10] W. Sobha, “Electrooptic and dielectric investigation on some liquid crystals.,” (thesis, Raman Research Institute, 1998).

[11] V. Manjuladevi, N. V. Madhusudana, to be published. (Raman Research Institute).

[12] B. S. Srikanta and N. V. Madhusudana, “Effect of skewed cybotactic structure on the dielectric constants and conductivities of some binary mixtures exhibiting the nematic phase.,” Mol. Cryt. Liq. Cryst. **103**, 111 (1983).

[13] L. Moodithaya, “Optical and elastic properties of liquid crystals.,” (thesis, Raman Research Institute, 1981).

[14] I. Haller, H. A. Huggins, H. R. Lilienthal, T. R. McGuire, “Ordered-related properties of some Nematic Liquids.,”, J. Phys. Chem. (USA) **77**, 950 (1973).

[15] D. A. Dunmur, and K. Szumilin “Field quenching of director fluctuations in thin films of nematic liquid crystals.,” Liq. Cryst. **6**, 449 (1989).

[16] J. V. Selinger and D. R. Nelson, “Density functional theory of nematic and smectic-A order near surfaces.,” Phys. Rev. A, **37**, 1736 (1988).

[17] D. A. Dunmur, A. Fukuda and G. R. Luckhurst, “Liquid Crystals: Nematics.,” (An Inspec Publication), pp-100. (R. Seelinger, H. Haspeklo, F. Noaek, Mol. Phys. (UK) **49**, 1039 (1983); L. G. P. Dalmolen, S. J. Picken. A. F. de Jong, W. H. de Jeu, J. Phys (France) **46**, 1443 (1985).

[18] E. F. Grasmbergen, L. Longa and W. H. de Jeu, “Landau theory of the isotropic-nematic phase transitions.,” Phys. Rep. **135**, 195 (1986).

[19] U. Finkenzeller, T. Geelahaar, G Weber and L. Phol “Liquid Crystalline reference compounds.,” Liq. Cryst. **5**, 313 (1989).

[20] N. Schopohl and T. J. Sluckin, “Defect core structure in nematic liquid crystals.,” Phys. Rev. Lett. **59**, 2582 (1987).